Electronic properties of carbon nanotubes calculated from density functional theory and the empirical π-bond model

**Deep Shah · Nicolas A. Bruque · Khairul Alam ·
Roger K. Lake · Rajeev R. Pandey**

Abstract The validity of the DFT models implemented by FIREBALL for CNT electronic device modeling is assessed. The effective masses, band gaps, and transmission coefficients of semi-conducting, zigzag, $(n, 0)$ carbon nanotubes (CNTs) resulting from the *ab-initio* tight-binding density functional theory (DFT) code FIREBALL and the empirical, nearest-neighbor π-bond model are compared for all semiconducting n values $5 \leq n \leq 35$. The DFT values for the effective masses differ from the π-bond values by $\pm 9\%$ over the range of n values, $17 \leq n \leq 29$, most important for electronic device applications. Over the range $13 \leq n \leq 35$, the DFT bandgaps are less than the empirical bandgaps by 20–180 meV depending on the functional and the n value. The π-bond model gives results that differ significantly from the DFT results when the CNT diameter goes below 1 nm due to the large curvature of the CNT. The π-bond model quickly becomes inaccurate away from the bandedges for a $(10, 0)$ CNT, and it is completely inaccurate for $n \leq 8$.

Keywords FIREBALL · CNT · DFT · NEGF · Bandstructure

1 Introduction

Carbon nanotube (CNT) systems are of high research interest for use in sensing and nanoelectronics. Electronic device

D. Shah · N.A. Bruque (✉) · K. Alam · R.K. Lake · R.R. Pandey
Department of Electrical Engineering, University of California, Riverside, CA 92521-0204, USA
e-mail: nbruque@ee.ucr.edu

R.K. Lake
e-mail: rlake@ee.ucr.edu

and circuit architecture concepts for bio-assembled CNTs have been described and demonstrated [1–5]. One system that we have found particularly interesting is a molecule joining two semiconducting CNTs. Such a system can display the electrical response of a resonant tunnel diode (RTD) [6–9], and we refer to it as a CNT-Mol-RTD.

The current-voltage response of a CNT-Mol-RTD depends on the alignment of the CNT bandedges with molecular states of the organic group [6–8]. Therefore, quantitative simulations of such a structure require models which are suitable for calculating the electronic states of both semiconductors, molecules, and the chemical bonds between the molecule and semiconductor. The models should be general enough to treat local distortions in the semiconductor lattice and distortion of the molecule. A CNT-Mol-RTD structure tends to be large compared to the benzene dithiol type of molecules that have been so heavily studied for molecular electronics [10–16]. Therefore, the model and its implementation must have the ability to handle large systems.

One model widely used for computational molecular electronics is density functional theory (DFT). DFT is a general, flexible theory with a proven record of calculating the electronic states of both semiconductors and molecules. The well known weakness of DFT implemented with widely used density functionals is its underestimation of the bandgap of semiconductors [17]. For electronic device modeling, this is not a trivial issue. The most famous example is that of Ge which is predicted within the local density approximation (LDA) or generalized gradient approximation (GGA) to be a metal. Another example is Zener tunneling which is exponentially dependent on the bandgap. It is this process that limits the maximum on-off current ratio in CNT field effect transistors. Linear errors in the bandgap result in exponentially large errors in the simulated minimum off-current [18]. The final example is the electron current of

a CNT-Mol-RTD. It depends on the alignment of a molecular state with the conduction band edge of the CNT. If the conduction band edge is too low, the predicted current—voltage response will be inaccurate. While hybrid functionals that include exact exchange greatly improve the situation, they also significantly increase the computational burden [19].

Another option for the simulation of large structures is to use empirical models [20, 21]. Such models can reproduce the bandgaps and energy levels of semiconductors with high accuracy. However, simulations of heterogeneous CNT, metal, organic, biological systems are difficult with empirical models due to issues of transferability of parameters. Conversely, electronic device simulations of semiconductors are difficult with DFT models due to the underestimation of the bandgap. One is forced to make a choice, and we have chosen the DFT model as implemented by the code FIREBALL [22, 23] since it has demonstrated the ability to model large biological molecules [24].

In this paper, we compare predictions of the properties relevant to electronic device modeling of semiconducting $(n, 0)$ CNTs calculated from both DFT theory and an empirical, tight-binding, π-bond model. Two important band-edge properties are the bandgap and the effective masses. For larger diameter CNTs, the empirical, tight-binding model is expected to predict the bandgap and band-edge effective masses with good accuracy since the empirical parameters have been chosen by fitting to those quantities. Therefore, for the larger diameter CNTs, we use the values of the bandgap and effective masses obtained from the π-bond model to assess the values obtained from the DFT model. For smaller diameter CNTs where the curvature becomes significant, the π-bond model breaks down.

Bandedge quantities alone are not sufficient for electronic device modeling. Since electronic devices are operated at biases on the order of a volt, accurate modeling of the higher energy states away from the bandedges is necessary for device modeling. The quantity that best characterizes the higher energy spectra for device simulations is the transmission coefficient. Therefore, we compare transmission coefficients calculated from the DFT and the empirical, tight-binding models.

Below, we calculate and compare the bandgaps, effective masses, and transmission spectra of semiconducting zigzag CNTs, ranging from $(5, 0)$ to $(35, 0)$ corresponding to diameters ranging from 0.39 nm to 2.8 nm. The bandgaps and effective masses are calculated, plotted, and compared for every non-metallic $(n, 0)$ CNT with $5 \leq n \leq 35$. Selected transmission coefficients are plotted and compared for $n = 10, 20, 31$, and 35.

2 Method of calculation

The FIREBALL calculations are performed using the local density approximation (LDA) (the Ceperley-Alder [25] form as parameterized by Perdew and Zunger [26]) and the BLYP exchange-correlation functional [27, 28]. A self-consistent calculation is performed using a generalization of the Harris-Foulkes [29, 30] energy functional referred to as DOGS after the authors of the original paper [31, 32]. A separable non-local pseudopotential [33] and a minimal sp^3 FIREBALL basis are used. The localized pseudoatomic orbitals are slightly excited due to hard wall boundary conditions imposed at certain cutoffs, r_c^{2s} and r_c^{2p} [32]. An excitation energy of approximately 2.0 eV is used to preserve the chemical bonding trends of carbon which results in $r_c^{2s} = 4.0$ Å and $r_c^{2p} = 4.5$ Å. Further details are given in [23].

After the FIREBALL DFT calculation finishes, the device Hamiltonian matrix elements, the overlap matrix, and the device-to-contact coupling matrices are extracted. The spatial extent of the non-zero matrix elements (the sparsity of the matrices) is determined by the pseudopotential cutoff limits and the FIREBALL orbital radii. Each CNT system, pictured in Fig. 1, consists of one CNT unit cell composed of 4 atomic layers periodically repeated in the axial direction. Non-zero matrix elements of a given atomic layer extend to the left and right 4 atomic layers, or one unit cell of the zigzag CNT. In terms of the 4-atomic layer unit cells, there is only nearest neighbor unit-cell coupling.

Transmission is calculated using the non-equilibrium Green function formalism (NEGF). The CNT is partitioned
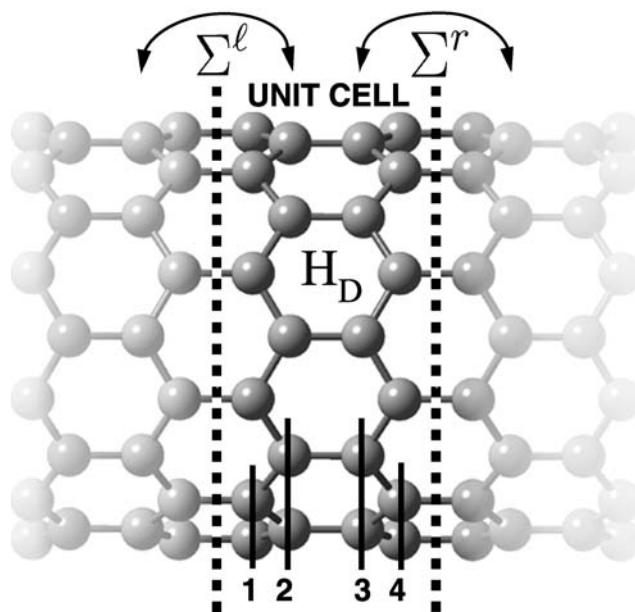

Fig. 1 One unit cell (10,0) zigzag CNT with 4 atomic layers. Self-energies take into account the semi-infinite leads for transmission calculations

into a "device" consisting of one unit cell and a left and right "contact." The left and right "contacts" are taken into account exactly by self-energies Σ^ℓ and Σ^r, respectively, as illustrated in Fig. 1. Details of the NEGF algorithm are described in [6–8].

For the empirical π-bond model, we use a nearest-neighbor model with matrix element $V_{pp\pi} = -2.77$ eV and $\epsilon_p = 0.0$ eV [34]. The NEGF algorithm is the same as that used with the FIREBALL matrix elements. The effective mass for both models is calculated from the 1-D dispersion using $1/m* = \frac{1}{\hbar^2} \partial^2 E / \partial k^2$. The energy band gap is determined from an $E - k$ calculation by reading the difference between the highest occupied band energy and the lowest unoccupied band energy at the Γ point.

3 Result and discussion

Figure 2a compares the calculated band gaps for $(n, 0)$ CNTs with $5 \leq n \leq 35$ leaving out the metallic CNTs with n values that are integer multiples of 3. The n values are shown on the bottom horizontal axis and the corresponding CNT diameters are shown on the top horizontal axis. On the plot itself, the data points indicate the n values for which calculations were performed. All other n values in that range correspond to metallic CNTs. At first glance, the bandgaps
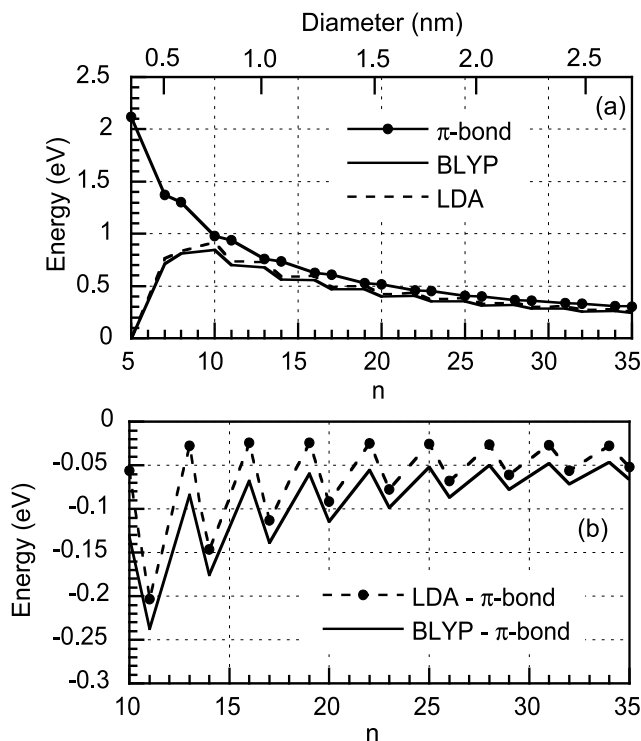
Fig. 2 **a** $(n, 0)$ CNT band gaps as a function of n and diameter calculated from the π-bond model and DFT with LDA and BLYP functionals. **b** Difference between the band gap calculated from the DFT models and the π-bond model

that result from the FIREBALL calculations closely track the bandgaps determined by the π-bond model for $n \geq 10$. CNTs in this size range are the ones that are most commonly synthesized, and they are the ones that are most important for electronic devices [35]. Below $n = 10$, the π-bond model breaks down due to the large curvature of the CNT. For the smallest CNT with $n = 5$, the FIREBALL calculations show zero bandgap. Upon closer inspection of Fig. 2a, one notices a sawtooth shape to the plot of bandgap versus n for the DFT calculations. We observe that the bandgap resulting from the DFT calculations corresponds closely to the bandgap resulting from the π-bond model for $(n, 0)$ CNTs when $n = 3p + 1$ where p is an integer ≥ 3.

This is shown clearly in Fig. 2b in which we plot the differences between the bandgaps calculated from the LDA and BLYP functionals and those from the π-bond model for $n \geq 10$. For $n = 3p + 1 \geq 13$, the LDA model underestimates the bandgap by 24–28 meV. For these n values, the BLYP model underestimates the bandgap by 46–84 meV. For $n = 3p - 1$ with p an integer, the discrepancies between the bandgaps resulting from the DFT models and the π-bond model are larger. For values of $n = 3p - 1 \geq 14$, the LDA model underestimates the bandgap by 52–147 meV. For these n values, the BLYP model underestimates the bandgap by 66–176 meV.

Figures 3 shows calculations and comparisons of the electron and hole effective masses. The plots of the left column show calculations and comparisons of the electron effective mass, and the plots of the right column show calculations and comparisons of the hole effective mass. In each row consisting of two plots, the scale and range of values is identical to facilitate easy comparisons between the values for electrons and holes. The calculated electron and hole effective masses (normalized to the bare electron mass) are plotted in Figs. 3a and d, respectively, versus n for all semiconducting values in the range $7 \leq n \leq 35$. One immediately notices that all models result in very similar values of effective masses for both the electrons and holes. To discern the differences, we plot the difference of the mass values calculated from the DFT models and the pi-bond model in Figs. 3b and e for electrons and holes, respectively. In other words, Figs. 3b and e show the normalized difference values $(m^*_{\text{DFT}} - m^*_{\pi\text{-bond}})/m_0$. Note that on the mass difference plots, b and e, the n values range from 10–35 whereas on the mass plots, a and d, the n values range from 7–35. The range of n is reduced on the difference plots to keep the plotted range of differences small. The difference plots show that the effective mass determined from the BLYP model tends to be larger than the effective mass determined by the LDA model. Over the range of n values $14 \leq n \leq 35$, the mass determined by the BLYP model has a maximum difference from the mass determined from the LDA model of 0.008 at $n = 14$ and a minimum difference of 0.002 at $n = 34$.
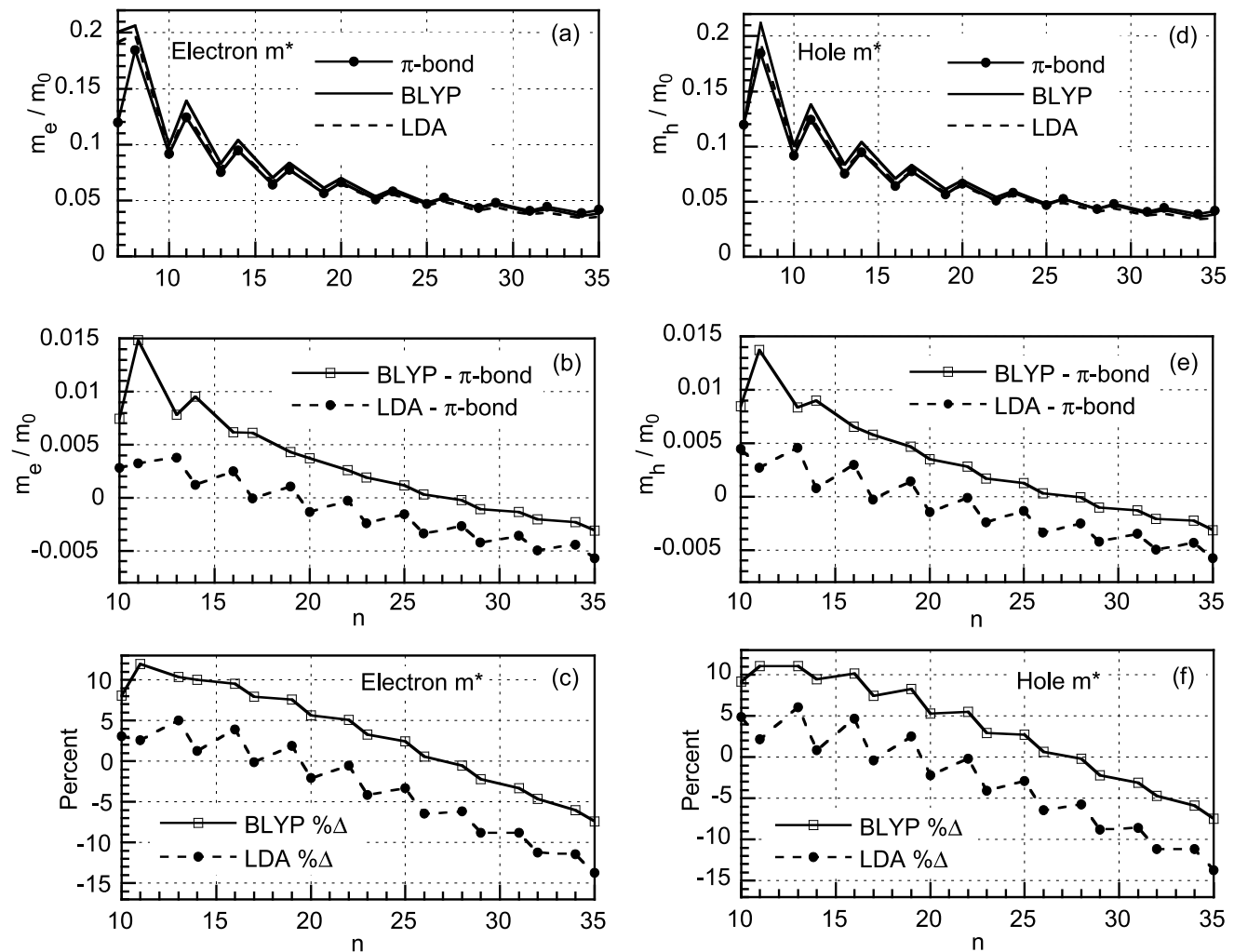
Fig. 3 Electron, (**a**)–(**c**), and hole, (**d**)–(**f**), effective mass comparisons. *Top*: Normalized effective mass (m^*/m_0), calculated from the π-bond and DFT models. *Middle*: Difference between the effective mass calculated from the DFT models and the π-bond model $(m_{\mathrm{DFT}} - m_{\pi-\mathrm{bond}})/m_0$. *Bottom*: Percent difference, $100 * (m_{\mathrm{DFT}} - m_{\pi\text{-bond}})/m_{\pi\text{-bond}}$

Also, the sawtooth peaks in the difference curves are out of phase with the sawtooth peaks in the mass curves above. The maximum differences occur at the minimums of the mass curves. Overall, the differences in the mass values predicted by the DFT models and the π-bond model are relatively small. To quantify the differences, the percent differences, $100 * (m_{\mathrm{DFT}} - m_{\pi\text{-bond}})/m_{\pi\text{-bond}}$, are plotted in (c) and (f). Over a wide range of the most useful n values for device applications, $17 \leq n \leq 29$, the values for the effective masses from the DFT models fall to within $+8\%$ to -9% of the values from the π-bond model.

So far, we have considered bandedge properties of bandgaps and effective masses. As we noted above, the higher energy electronic spectra is also important for electronic device modeling, and the best way to characterize it is to calculate the transmission coefficients. Figure 4 shows the transmission spectra for $(10, 0)$, $(20, 0)$, $(31, 0)$ and $(35, 0)$

CNTs calculated using DFT/BLYP, DFT/LDA, and the empirical, π-bond model. In all cases, the energy axis of the transmission curves has been shifted such that the center of the bandgap lies at 0 eV. The energy region in Fig. 4 for which the transmission is zero is the band gap for the CNTs.

For the 2 largest CNTs, $n = 31$ and 35, the transmission resulting from the DFT and π-bond models all have similar, symmetric forms. There is some compression of the energy scale for the transmission coefficients calculated from the DFT models compared to the transmission coefficient calculated from the π-bond model. The energy separation between higher modes is smaller in the DFT models then in the π-bond model.

For the smallest CNT, $n = 10$, there is a noticeable, qualitative difference between the transmission calculated from the DFT models and the π-bond model. The transmission resulting from the π-bond model is always symmetric around
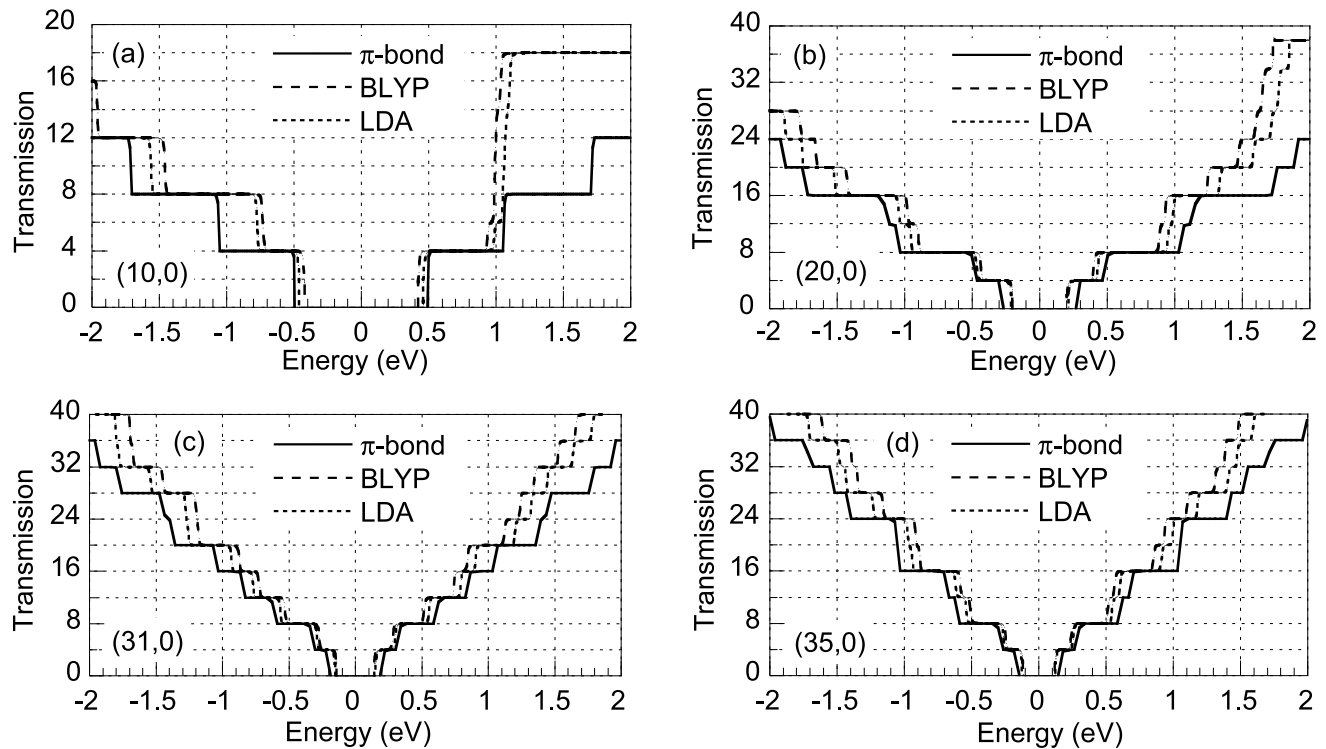
Fig. 4 Transmission calculated from π-bond and DFT models for $(n, 0)$ CNTs with n values of **a** 10, **b** 20, **c** 31, and **d** 35

the center of the bandgap. For the DFT models, the transmission is noticeably asymmetric. Approximately 0.5 eV above the conduction band edge, the DFT models predict 3 bands closely spaced and 2 bands doubly degenerate. These 7 bands, multiplied by 2 for spin, give rise to the large step of 14 in the transmission coefficient 0.5 eV above the conduction band edge in the transmission coefficient of the $(10, 0)$ CNT. This large increase in the transmission and density of states 0.5 eV in the conduction band is significant for device modeling. A similar large step is also observed in a transmission calculation based on the SIESTA code for a $(7, 0)$ CNT [36]. A similar large increase in the transmission also occurs in the $(20, 0)$ CNT at 1.3 eV above the conduction band edge.

The differences in the $(10, 0)$ valence band transmission resulting from the DFT and π-bond models, while not as dramatic as those in the conduction band, are still significant from a device modeling perspective. The 0.5 eV gap between the valence band edge and the next lower pair of bands found from the π-bond model is reduced to approximately 0.3 eV in the DFT models. These energies lie within the applied voltage window, (V_{DD}), of any of the most optimistically scaled CNT field effect transistors, and will, thus, affect the physics of the carrier transport. While our main focus is on assessing the validity of the DFT models for device modeling, these results also provide an assessment of

the π-bond model and show that the π-bond model should be used with care and scepticism for $(10, 0)$ CNTs.

4 Summary

The goal of this work is to assess the validity of the DFT models implemented by FIREBALL for CNT electronic device modeling. Our approach is to compare the electronic properties resulting from the DFT models with those resulting from the π-bond model since the parameters of the π-bond model have been empirically chosen to give a good fit to the bandgap and effective mass for CNTs with diameters that are "not too small." We have compared the bandgaps, effective masses, and transmission coefficients of $(n, 0)$ CNTs calculated from the empirical π-bond model, DFT/LDA, and DFT/BLYP models.

For values of n in the range $17 \leq n \leq 29$, the calculated effective masses from the DFT models are within $\pm 9\%$ of those calculated from the π-bond model. For $n \geq 10$, the difference between the bandgap calculated from the π-bond model and the bandgaps calculated from the DFT models oscillates as a function of n. The differences are smallest for $n = 3p + 1$ where p is an integer, and the differences are largest for $n = 3p - 1$. For $n = 3p + 1 \geq 13$, the LDA model underestimates the bandgap by 24–58 meV and the BLYP model underestimates the bandgap by 46–84 meV.

For $n = 3p - 1 \geq 14$, the LDA model underestimates the bandgap by 52–147 meV and the BLYP model underestimates the bandgap by 66–176 meV. Overall, in the important range of n values most relevant for CNT devices, $17 \leq n \leq 29$, the bandgaps, effective masses, and transmission coefficients calculated from the DFT models implemented by FIREBALL are sufficiently accurate for electronic device simulations.

These simulations also quantify what is meant by "not too small" when applying the π-bond model. For $n = 10$, the bandedge properties resulting from the π-bond and DFT models agree to within 10%, however, the π-bond model quickly becomes inaccurate away from the bandedges. The transmission from the higher energy modes resulting from the π-bond model has differences with those resulting from the DFT models which are significant for device modeling. For $n \leq 8$, the π-bond model is completely inaccurate.

References

1. Keren, K., Berman, R.S., Buchstab, E., Sivan, U., Braun, E.: Sci. **302**, 1380 (2003)
2. Braun, E., Keren, K.: Adv. Phys. **53**, 441 (2004)
3. Williams, K.A., Veenhuizen, P.T.M., de la Torre, B.G., Eritja, R., Dekker, C.: Nat. **420**, 761 (2002)
4. den Dulk, R., Williams, K.A., Veenhuizen, P.T.M., de Konig, M.C., Overhand, M., Dekker, C.: In: Fritzsche, W. (ed.) DNA-Based Molecular Electronics, vol. 725, pp. 25–31. AIP, New York (2004)
5. Dwyer, C., Johri, V., Cheung, M., Patwardhan, J., Lebeck, A., Sorin, D.: Nanotechnol. **15** 1240 (2004)
6. Bruque, N., Pandey, R.R., Lake, R., Wang, H., Lewis, J.: Mol. Simul. **31**, 859 (2005)
7. Pandey, R.R., Bruque, N., Alam, K., Lake, R.: Phys. Stat. Sol. (a) **203**, R5 (2006)
8. Bruque, N.A., Alam, K., Pandey, R.R., Lake, R.K., Lewis, J.P., Wang, X., Liu, F., Ozkan, C.S., Ozkan, M., Wang, K.L.: J. Nanoelectron. Optoelectr. **1**, 74 (2006)
9. Wang, X., Liu, F., Andavan, G.T.S., Jing, X., Bruque, N., Pandey, R.R., Lake, R., Singh, K., Ozkan, M., Wang, K.L., Ozkan, C.S.: Small **2**, 1356 (2006)
10. Damle, P., Ghosh, A., Datta, S.: Phys. Rev. B **64**, 201403 (2001)
11. Damle, P., Ghosh, A.: Datta. S.: Chem. Phys. **281**, 171 (2002)
12. Rakshit, T., Liang, G., Ghosh, A., Datta, S.: Nano Lett. **4**, 1083 (2004)
13. Xue, Y., Datta, S., Ratner, M.A.: Chem. Phys **281**, 151 (2002)
14. Xue, Y., Datta, S., Ratner, M.A.: J. Chem. Phys. **115**, 4292 (2001)
15. Yaliraki, S.N., Ratner, M.A.: J. Chem. Phys. **109**, 5036 (1998)
16. Seminario, J.M., Cordova, L.E., Derosa, P.A.: Proc. IEEE **91** 1958 (2003)
17. Martin, R.M.: Electronic Structure Basic Theory and Practical Methods. Cambridge University Press, Cambridge (2004)
18. Alam, K., Lake, R.K.: Appl. Phys. Lett. **87**, 073104 (2005)
19. Muscat, J., Wander, A., Harrison, N.M.: Chem. Phys. Lett. **342**, 397 (2001)
20. Canning, A., Wang, L.W., Williamson, A., Zunger, A.: J. Comp. Phys. **160**, 29 (2000)
21. Klimeck, G., Oyafuso, F., Boykin, T.B., Bowen, R.C., von Allmen, P.: CMES-Comput. Model. Eng. Sci. **3**, 601 (2002)
22. Sankey, O.F., Niklewski, D.J.: Phys. Rev. B **40**, 3979 (1989)
23. Lewis, J.P., Glaesemann, K.R., Voth, G.A., Fritsch, J., Demkov, A.A., Ortega, J., Sankey, O.F.: Phys. Rev. B **64**, 195103 (2001)
24. Lewis, J.P., Starikov, T.E.C. III E.B., Wang, H., Sankey, O.F.: J. Phys. Chem. B **107**, 2581 (2003)
25. Ceperley, D.M., Alder, G.J.: Phys. Rev. Lett. **45**, 566 (1980)
26. Perdew, J.P., Zunger, A.: Phys. Rev. B **23**, 5048 (1981)
27. Becke, A.D.: Phys. Rev. A **38**, 3098 (1988)
28. Lee, C., Yang, W., Parr, R.G.: Phys. Rev. B **37**, 785 (1988)
29. Harris, J.: Phys. Rev. B **31**, 1770 (1985)
30. Foulkes, W.M.C., Haydock, R.: Phys. Rev. B **39**, 12520 (1989)
31. Demkov, A.A., Ortega, J., Sankey, O.F., Grumbach, M.P.: Phys. Rev. B **52**, 1618 (1995)
32. Sankey, O.F., Demkov, A.A., Windl, W., Fritsch, J.H., Lewis, J.P., Fuentes-Cabrera, M.: Int. J. Quantum Chem. **69**, 327 (1998)
33. Hamann, D.R.: Phys. Rev. B **40**, 2980 (1989)
34. Mintmire, J.W., Robertson, D.H., White, C.T.: J. Phys. Chem. Solids **54**, 1835 (1993)
35. Chen, Z., Appenzeller, J., Knoch, J., Lin, Y.-M., Avouris, P.: Nano Lett. **5**, 1497 (2005)
36. Adessi, C., Roche, S., Blase, X.: Phys. Rev. B **73**, 125414 (2006)